MULTI-BAND RADIO-FREQUENCY INTEGRATED CIRCUITS FOR MULTIBAND AND MULTIMODE WIRELESS COMMUNICATION, RADAR AND SENSING SYSTEMS IN HARSH ENVIRONMENTS

Cuong Huynh, Jaeyoung Lee, and Cam Nguyen

Department of Electrical and Computer Engineering
Texas A&M University
College Station, Texas 77843, U.S.A.

ABSTRACT

Some recently developed 0.18-µm SiGe BiCMOS radio-frequency integrated circuits (RFICs) for multiband multimode wireless communications, radar and sensing systems, which provides many benefits for sensing and communications in uncertain environments with harsh operational scenarios, are presented. The multiband low-noise amplifier has measured peak gain of 21.9/16.6 dB at 23.5/35.7 GHz and best measured noise figure of 5.1/7.2 dB at 22/35.6 GHz, respectively. The multiband power amplifier exhibits gain of 21.4 and 17 dB, maximum output power of 16 and 13 dBm, and maximum power add efficiency (PAE) of 10.6 % and 4.9 % at 25.5 and 37 GHz respectively. The ultra-wideband pulse generator exhibits -1.9 dB (loss) to 1.1 dB (gain) from 31 to 37.1 GHz and produces very narrow RF pulses of 200 ps with extremely low RF leakage. The up-conversion mixer exhibits a conversion gain of 25.7 dB, 1-dB input power of -23 dBm, 1-dB output power of 1.36 dBm, and maximum output power of 2.7 dBm at 24.5 GHz.

Index Terms—RFIC, multi-band systems, multi-band components, harsh sensing and communication environment.

1. INTRODUCTION

Advanced communication, radar and sensing systems working "concurrently" over multiple bands and/or multi-mode provide numerous advantages and have more capabilities as compared to their single-band/single-mode counterparts for communications and sensing - a fact that is simple to understand since the communication and sensing are performed at multiple frequencies and/or multiple modes simultaneously. The ability of operating multiple bands/modes simultaneously increases the diversity of transmitters and receivers and hence systems for simultaneous communications or sensing at multiple frequencies/modes – especially needed when operating in uncertain environments accompanied with harsh operational scenarios such as severe multi-path fading, such as indoors, urban settings or mountainous terrains, or when signal attenuation at some frequencies are excessively high, which hinder the communication and sensing capabilities. Multi-band Radio-Frequency Integrated Circuits (RFICs) are the backbone of modern multiband multimode wireless communication, radar and sensing systems, enabling low-cost, small-size, and high-performance single-chip solution. In this talk, we will present some of the recent developments of RFICs for multiband multimode wireless communications, radar and sensing, which can enhance the sensing and communications in uncertain harsh environments. Specifically, the presented RFICs are parts of a millimeter-wave dual-band dual-mode radar array system designed for sensing in complex urban environments and structures having harsh operations.

2. MULTI-BAND LOW-NOISE AMPLIFIER

Various concurrent multiband low-noise amplifiers (LNAs) have been developed. Most developed concurrent multiband LNAs, however, have been aimed for RF applications below 10 GHz due to their large market share and interests. In the high RF range of microwave and millimeter-wave (mm-wave) frequencies exceeding 10 GHz, there are still many challenges in developing concurrent multiband LNAs in silicon technology, such as limited gain due to low f_T and f_{max} of transistors, high loss due to silicon substrate, low inductor and transmission-line quality (Q) factors, and inadequate modeling of integrated inductors, etc. In order to compensate for the low Q-factor of inductors, several alternative techniques employed in concurrent multiband LNAs have been reported – for instance, feedback [1] and synthetic [2] transmission lines, active notch filters [3], and feedback notch filters [4]. Among the proposed techniques, the active notch filter is an attractive solution for creating stop-bands because it can achieve a narrower and deeper stop-band notch response (high Q-factor) by compensating for the resistive loss of an inductor with its negative resistance. The active notch filters have been developed and widely used for image/interference rejection LNAs for RF and lower microwave applications [5]. However, they have

978-1-4799-2893-4/14/$31.00 ©2014 IEEE

rarely been implemented for high microwave and mm-wave applications. In this section, we present a new 24/35-GHz concurrent dual-band LNA using a new active notch filter in a 0.18-µm SiGe BiCMOS technology [6].

Fig. 1 shows the die microphotograph of the concurrent dual-band LNA occupying an area of 490 μm × 390 μm. Fig. 2 shows the simulated and measured results. The dual-band LNA has peak gain of 21.9/16.6 dB at 23.5/35.7 GHz, respectively. The best noise figure is obtained as 5.1/7.2 dB at 22/35.6 GHz, respectively. The measured IIP_3 performances are -10.4/-8.3 dBm at 24/35 GHz, respectively.

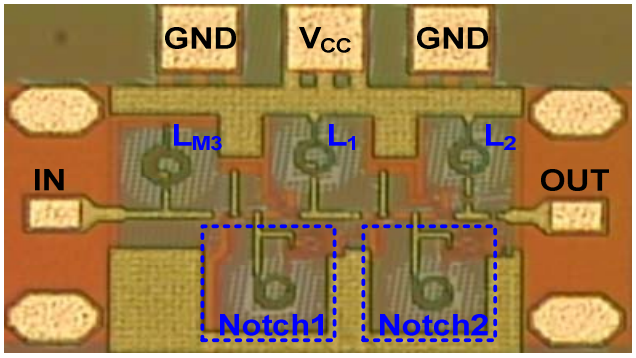

Fig. 1. Die photograph of the concurrent dual-band LNA.

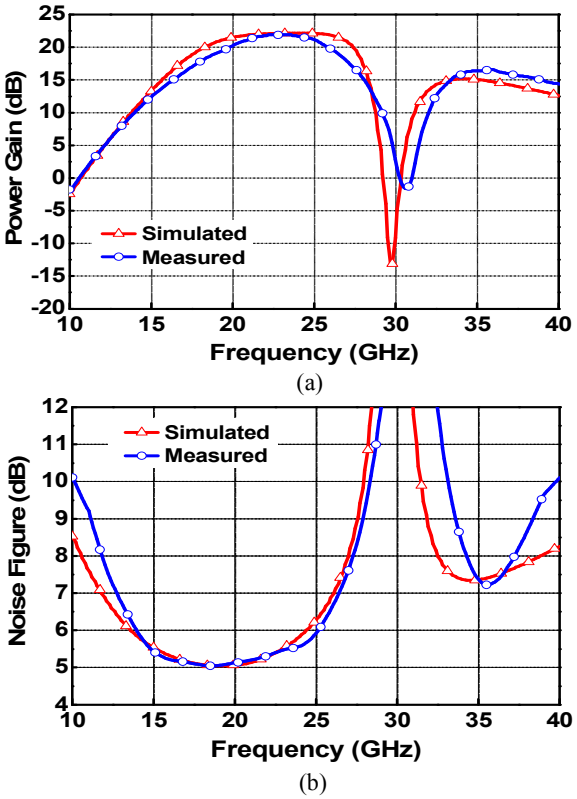

Fig. 2. Simulated and measured results for (a) power gain and (b) noise figure of the concurrent dual-band LNA.

3. MULTI-BAND POWER AMPLIFIER

Several multiband power amplifiers (PAs) working to 5.2 GHz using concurrent multiband matching networks were reported [7]-[10]. This section describes a new dual-band PA working concurrently at 25.5 and 37 GHz designed using a concurrent dual-band matching technique.

Fig. 3 shows a microphotograph of the dual-band PA designed using a 0.18-µm SiGe BiCMOS technology [6]. It has a chip area of 1.3 × 0.68 mm^2. Fig. 4 shows the simulated and measured gain, input and output return loss, and reverse isolation of the concurrent dual-band PA under small-signal conditions. The dual-band PA exhibits gains of 21.4 dB and 17 dB, 3-dB bandwidths of 3.7 GHz and 1.8 GHz, input return losses of 14.8 and 9 dB, and output return losses of 12.5 and 15 dB at 25.5 GHz and 37 GHz, respectively. The reverse isolation is higher than 35 dB from DC to 55 GHz.

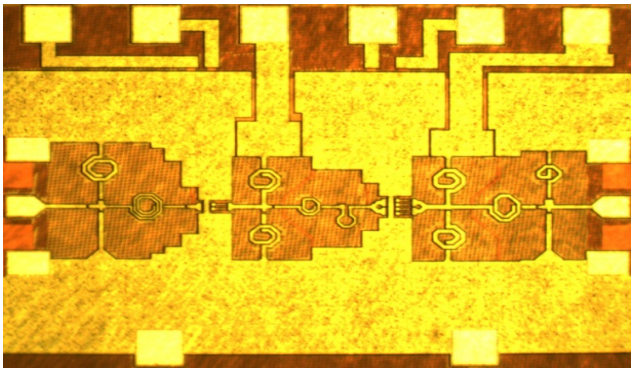

Fig. 3 Microphotograph of the 25.5/37-GHz dual-band PA.

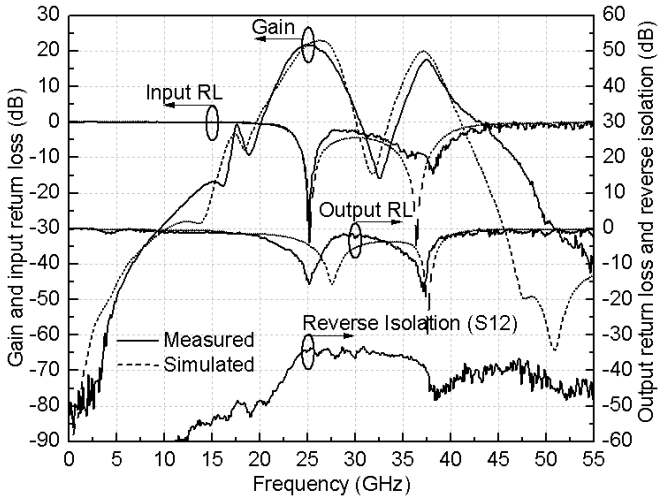

Fig. 4 Measured and simulated small-signal gain, return loss, and reverse isolation.

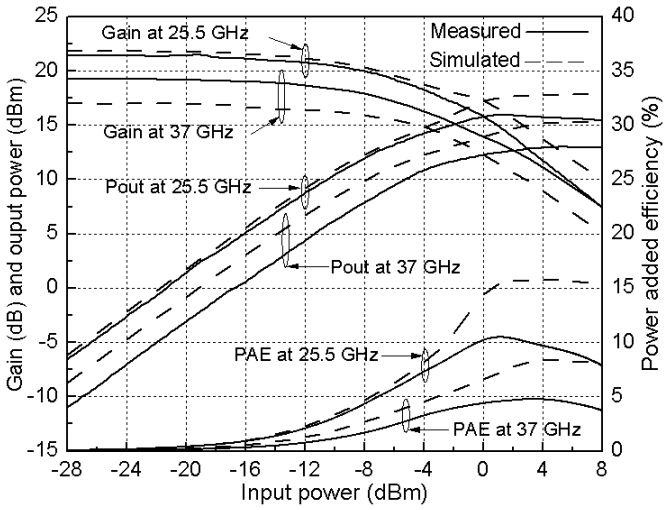

Fig. 5 Measured and simulated gain, output power and PAE at 25.5 and 37 GHz.

Fig. 5 shows the measured and simulated gain, output power and the power added efficiency (PAE) at 25.5 and 37 GHz. The measured results show that the maximum output powers, $P_{out,max}$, reach 16 and 13 dBm, output 1-dB compression points, $P_{out,1dB}$, are 10.4 and 7.1 dBm, and maximum PAEs, PAE_{max}, are 10.6 and 4.9 % at 25.5 and 37 GHz, respectively.

4. ULTRA-WIDEBAND RF PULSE GENERATOR

Ultra-wideband pulse generators are needed for single-band and multi-band RF systems. A SiGe SPST switch used as RF pulse generator in automotive radar systems has been reported in [11]. This SPST switch uses the current steering technique and exhibits 0-dB gain and 35-dB isolation at 24 GHz, and 70-ps rising and falling times. The isolation of this RF-pulse former is limited by the inherent parasitic components of the transistors at high frequencies and it consumes a high dc power from a 5-V power supply. This section presents a Ka-band low-power RF pulse generator designed using a 0.18-µm SiGe BiCMOS technology [6], exhibiting very fast switching speed, extremely low RF leakage, and very narrow RF pulse.

Fig. 6 shows a microphotograph of the RF pulse generator with a chip area of 450 x 500 μm^2 and its simulated and measured insertion loss/gain, input and output return losses, and isolation under small signal conditions. The measured results show that, around the design frequency of 35 GHz, the RF pulse generator exhibits an ultra-high-isolation performance, hence extremely low RF leakage. From 31 to 37.1 GHz, the loss/gain is from -1.9 dB (loss) to 1.1 dB (gain), the input return loss is from 14.5 to 30 dB. The output return loss is higher than 10 dB from 33 to 35.9 GHz. From 30 to 40 GHz the isolation is higher 40 dB and, especially at 34 GHz, the isolation reaches 70 dB along with the gain of 1.1 dB. Fig. 7 shows the measured 0.8-ns RF-pulses and its spectrum. There is no RF leakage seen from the measured spectrums; the leakage, if any, is smaller than the magnitude of the actual RF-pulse, which demonstrates the ultra-high isolation of the RF pulse generator. From Fig. 4(a), the 10%-90% rising time and 90%-10% falling time of the RF-pulse former are determined to be 136 ps and 70 ps, respectively. The small measured switching time of 206 ps allows the RF pulse generator to produce very narrow RF-pulses for high resolution radar and high-data-rate communication systems.

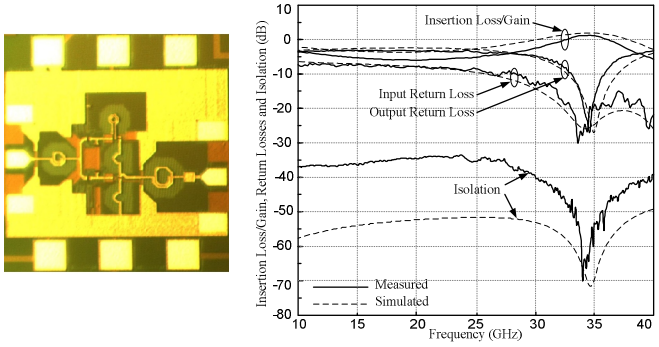

(a) (b)

Fig. 6. Microphotograph (a), and simulated and measured insertion loss/gain, return losses and isolation (b) of the RF pulse generator.

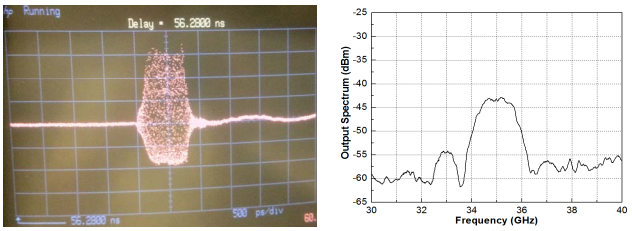

(a) (b)

Fig. 7. Measured 0.8-ns 35-GHz RF-pulse (a) and its spectrum (b).

5. UP-CONVERSION MIXER

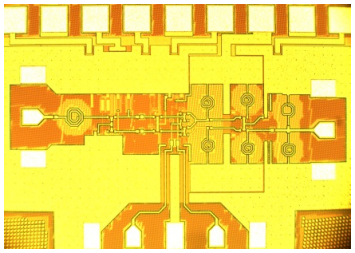

Fig. 8. K-band mixer microphotograph.

This section presents an up-conversion mixer in K-band designed using a 0.18-µm SiGe BiCMOS technology [6] that fully integrates a double-balanced Gilbert mixer cell [12] with an active balun, differential amplifier and band-

pass filter. Fig. 8 shows a microphotograph of the K-band

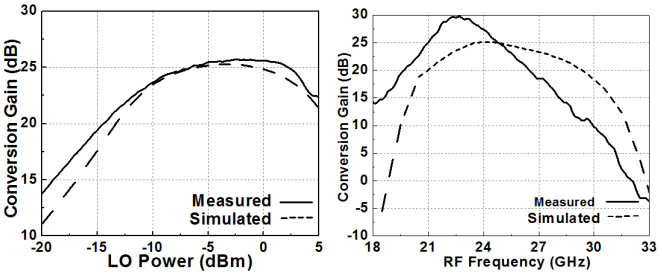

(a) (b)

Fig. 9. (a) Measured and simulated conversion gain versus LO power. (b) Measured and simulated conversion gain versus RF frequency.

mixer having a size of 1.2 mm x 0.9 mm.

Fig. 9(a) shows the simulated and measured conversion gains versus LO power. The frequency and power of IF signal are set to 21 GHz and -40 dBm, respectively. The LO frequency is fixed at 3.5 GHz and the LO power is swept from -20 to 5 dBm with the step of +1 dBm. The measured result shows that the maximum conversion gain of 25.7 dB is obtained with the LO power of -2 dBm. Fig. 9(b) shows the conversion gain versus the RF frequency with -2 dBm LO power. The 5-dB RF bandwidth is from 21-25 GHz. The measured results show that the mixer exhibits a conversion gain of 25.7 dB at RF frequency of 24.5 GHz, and the maximum conversion gain of 29.5 dB is located at 22.5 GHz.

6. CONCLUSION

Various RFICs including multiband LNA and PA, ultra-wideband pulse generator, and up-conversion mixer, representing samples of our recently developed RFICs for multiband multimode wireless communication, radar and sensing systems, have been developed. These RFICs are components of a millimeter-wave dual-band dual-mode array system designed for sensing in complex urban environments and structures having harsh operational scenarios. The successful development of these RFICs with state-of-the-art performance facilitates the design of high-performance modern multiband multimode communication, radar and sensing systems that have many benefits, especially for applications involving uncertain harsh operating environments.

ACKNOWLEDGEMENT

This paper was made possible by NPRP grant # 6-241-2-102 from the Qatar National Research Fund (a member of Qatar Foundation). The statements made herein are solely the responsibility of the authors.

REFERENCES

[1] [2] H. S. Jhon, I. Song, J. Jeon, H. Jung, M. Koo, B.-G. Park, J. D. Lee and H. Shin, “8mW 17/24 GHz dual-band CMOS low-noise amplifier for ISM-band application,” IET Elec-tronics Letters, vol. 44, no. 23, pp. 1353–1354, Nov. 2008.

[2] K. A. Hsieh, H. S. Wu, K. H. Tsai, and C. K. C. Tzuang, “A dual-band 10/24-GHz amplifier design incorporating dual-frequency complex load matching,” IEEE Trans. Microw. Theory Tech., vol. 60, no. 6, pp. 1649–1657, June 2012.

[3] C. W. Ang, Y. Zheng, and C. H. Heng, “A multi-band CMOS low noise amplifier for multi-standard wireless receivers,” in IEEE Int. Symp. on Circuits and Systems Dig., 2007, pp. 2802–2805.

[4] J. Lee and C. Nguyen, “A 13/24/35-GHz concurrent tri-band LNA with feedback notches,” in IEEE Topical Meetings on Silicon Monolithic Integrated Circuits in RF Systems (SiRF) Dig., Jan. 2013, pp. 252–254.

[5] T.-K. Nguyen, N.-J. Oh, C.-Y. Cha, Y.-H. Oh, G.-J. Ihm, and S.-G. Lee, “Image-rejection CMOS low-noise amplifier design optimization techniques,” IEEE Trans. Microw. Theory & Tech., vol. 53, no. 2, pp. 538–547, Feb. 2005.

[6] Jazz Semiconductor, 4321 Jamboree Road, Newport Beach, CA 92660.

[7] M.R. Ghajar and S. Boumaiza, "Concurrent dual band 2.4/3.5 GHz fully integrated power amplifier in 0.13µm CMOS technology," Proceeding of EuMC, Rome, Italy, September 2009, pp. 375–378.

[8] S.-F. R. Chang, W. L. Chen, S. C. Chang, C. K. Tu, C. L. Wei, C. H. Chien, C. H. Tsai, J. Chen, and A. Chen, “A dual-band RF transceiver for multistandard WLAN applications,” IEEE Trans. Microw. Theory Tech., vol. 53, no. 3, pp. 1048–1055, Mar. 2005.

[9] P. Colantonio, F. Giannini, R. Giofre, and L. Piazzon, “A design technique for concurrent dual-band harmonic tuned power amplifier,” IEEE Trans. Microwave Theory and Tech., vol. 56, no.11, pp. 2545–2555, Nov. 2008.

[10] Wenhua Chen, Seyed Aidin Bassam, Xiang Li, Yucheng Liu, Karun Rawat, Mohamed Helaoui, Fadhel M. Ghannouchi, Zhenghe Feng, "Design and Linearization of Concurrent Dual-Band Doherty Power Amplifier With Frequency-Dependent Power Ranges", IEEE Trans. Microw. Theory Tech., vol. 59, no. 10, pp. 2537–2545, Oct. 2011.

[11] I. Gresham and A. Jenkins, “A fast switching, high isolation absorptive SPST SiGe switch for 24 GHz automotive applications,” presented at the 33rd Eur. Microwave Conf., Munich, Germany, 2003.

[12] B. Gilbert, “A precise four quadrant multiplier with subnanosecond response,” IEEE J. Solid-State Circuits, vol. SC-3, no. 12, pp. 365–373, Dec. 1968.